**NASA TECHNICAL MEMORANDUM**

NASA TM X-71741

NASA TM X-71741



# TURBOFAN COMPRESSOR DYNAMICS DURING AFTERBURNER TRANSIENTS


by Anatole P. Kurkov
Lewis Research Center
Cleveland, Ohio 44135

TECHNICAL PAPER to be presented at
The Symposium on Unsteady Phenomena in Turbomachinery
sponsored by AGARD Propulsion and Energetics Panel
Monterey, California, September 22-26, 1975

# TURBOFAN COMPRESSOR DYNAMICS DURING AFTERBURNER TRANSIENTS

by
Anatole P. Kurkov
Lewis Research Center
National Aeronautics and Space Administration
Cleveland, Ohio 44135





## SUMMARY

The effects of afterburner light-off and shut-down transients on the compressor stability are investigated. The reported experimental results are based on detailed high-response pressure and temperature measurements on the TF30-P-3 turbofan engine. The tests were performed in an altitude test chamber simulating high-altitude engine operation. It is shown that during both types of transients, flow breaks down in the forward part of the fan-bypass duct. At a sufficiently low engine inlet pressure this resulted in a compressor stall. Complete flow breakdown within the compressor was preceded by a rotating stall. At some locations in the compressor, rotating stall cells initially extended only through part of the blade span. For the shutdown transient the time between first and last detected occurrence of rotating stall is related to the flow Reynolds number. An attempt was made to deduce the number and speed of propagation of rotating stall cells.

## INTRODUCTION

This paper describes the significant features of the flow field in the TF30-P-3 engine during afterburner transients, including the history of compressor stall. In a turbofan engine pressure waves originating as a result of either afterburner ignition or shut-down transients can propagate upstream through the fan-bypass duct and ultimately cause an instability in the compressor system. Previously reported results on the TF30-P-3 afterburner performance and engine operating limits, Ref. 1, indicated that afterburner transients restrict appreciably the stall-free engine operating envelope at a simulated flight Mach number of 1.4. The reported pressure histories throughout the engine during afterburner transients, furthermore, indicated fairly large pressure fluctuations in the vicinity of the splitter ring which separates the compressor-core flow from the fan-bypass flow. This investigation is an attempt to relate these phenomena to the engine internal flow field during transient operation by considering additional experimental data.

Additional information is also provided concerning the sequence of events within the compressor system leading to stall. Aside from providing documentation on an engine operational stall, information of this type is of a more general interest. For example, these processes also control engine response characteristics under time-variant inlet flow distortion.

The investigation was conducted in the altitude test facility over a range of simulated altitudes from 14.5 to 17.5 km (47 570 to 57 415 ft) and a flight Mach number of 1.3. These experimental results are based on high-response pressure and temperature data.

## APPARATUS AND PROCEDURE

### Engine

Figure 1 illustrates the engine and associated inlet ducting. Also indicated in the figure are the locations of instrumentation planes. The engine compressor system consists of a three-stage fan and a six-stage low-pressure compressor mounted on the common shaft, and a seven-stage high-pressure compressor mounted on a separate shaft. The flow at the fan exit is divided by means of a short splitter ring into the compressor-core and the fan-bypass streams. The Military sea-level static compressor pressure ratio is 17:1 with a bypass ratio of 1:1. A single-stage turbine drives the high-pressure compressor and a three-stage turbine drives the fan and the low-pressure compressor.

### Afterburner

The fuel in the afterburner is introduced through seven fuel spray rings divided into five zones. The fuel schedule for the afterburner is integrated with the exhaust nozzle area control. During afterburner ignition transient the nozzle area is opened in steps following the consecutive introduction of fuel into the five fuel spray zones. Exhaust nozzle is opened in order to compensate for the pressure increase in the afterburner due to combustion. The total time for the ignition transient is about 8.5 seconds. Afterburner shutdown is accomplished much faster; total time is about 2 seconds. No staging of fuel flow or the exhaust nozzle area is used in this transient. As a result of the control schedule and the dynamic characteristics of the exhaust nozzle control, during both transients the pressure in the afterburner initially increases. Additional information relating to afterburner design and the control schedule is given in Ref. 1.

### Instrumentation

The axial location of instrumentation planes is indicated in Fig. 1. Where two numbers are used to designate a station, the second number indicates the stage; i.e., station 2.3 is located behind the third fan stage. Stages are numbered consecutively starting with the first fan stage and ending with the last stage in the high pressure compressor. Addition of the letter F to the station number indicates that a particular station is located in fan-bypass duct. The exact positions of all of the high-response pressure transducers used in the investigation are indicated in Table I. The angles were measured in the direction of engine rotation, i.e., clockwise facing upstream. Zero degrees corresponded to the 12 o'clock position. Since all static pressures were measured at the outer wall of the passage (passage

height 100 percent), the first two numbers are sufficient to describe the position of each static pressure transducer. For a total pressure transducer, it is also necessary to specify its radial position using the fourth column. It is seen that the smaller the number in this column, the closer the transducer is to the outer wall. Thus, for example, 2-108 implies duct-wall static pressure measurement at the engine inlet 108 degrees from the 12 o'clock position; and 3-118-1 implies total pressure measurement at the low-pressure exit 118 degrees from the 12 o'clock position at a spanwise position closest to the tip wall.

The design of the pressure probes, their response characteristics, and calibration procedures are discussed in detail in Refs. 2 and 3. In general, the frequency response was about 300 Hz with maximum amplitude error of ±5 percent. Temperature was measured using 0.0076 cm (0.003 in.) Chromel-Alumel bare wire thermocouple probes. Locations of thermocouples used in the analyses are given in Table II. The time constant for these probes was typically of the order of 0.010 second. The high response pressure data were recorded on a magnetic tape and, simultaneously, on a high-speed digitizer-recorder. Temperature data were recorded only on the digital recorder, which was operated at a sampling rate of 20 samples per second per channel. The analysis of the compressor stall history was performed by digitizing and converting to engineering units the pressure data recorded on the magnetic tape.

## RESULTS

### Summary of Test Conditions

Figure 2 illustrates test conditions for each test point for which high-speed data were available. The simulated flight Mach number was 1.31±0.01. The flight altitude was calculated assuming Mach number 1.31 and assuming inlet pressure recovery of 0.985. Also indicated in the figure are the stall boundaries for each type of transient. On ignition, i.e., throttle movement from Military to Maximum, stall occurred when the Reynolds number index dropped below 0.23. For throttle excursion from Maximum to Military, the critical Reynolds number index was about 0.34. The detailed analysis of high-response data will be presented only for one test point, point 23; however, a summary of stall history will be also presented for the other four stall points indicated in Fig. 2. Detailed results were also obtained for points 25 and 28 which are seen to be just outside of the respective stall regions. However, only qualitative conclusions based on these results will be presented.

### Internal Flow Characteristics During Ignition Transient

Examination of stall pressure traces for points 23 and 24 and of the detailed afterburner schedule (Ref. 1) indicates that stall on ignition transient occurs when fuel is being introduced into the Zone 1 primary circuit. Therefore, the description of the internal flow field will be confined to this part of the ignition transient. The pressure traces during the transient for point 23 are presented in Fig. 3. Pressure histories in the fan-bypass duct and afterburner are included in Figs. 3(a) to (c). Most of the remaining pressures are given in Figs. 3(d) and (e), respectively, for the left and right sides of the engine. In these two figures, the absolute pressures are plotted in the same order as they appear in the engine starting with the engine inlet station 2 at the bottom and terminating with compressor stations 3.12 or 4 at the top. A different pressure scale is used for higher pressure levels starting with station 2.6. Whenever available, a neighboring static pressure is plotted next to a total pressure trace in order to provide an indication of the magnitude of velocity at a particular station. Static and total pressures are differentiated in Fig. 3 by using different line symbols and by the nomenclature defined in Table I.

The static pressure rise at station 8 in the afterburner, Fig. 3(a), is due to the ignition process. This pressure rise is closely followed by a static pressure rise in the fan duct at station 4F. However, at the fan exit, station 2.3F, total pressure fails to rise. In fact, it is seen that the total pressure at 111 degrees following ignition drops below the static pressure at 124 degrees, indicating a flow breakdown in this part of the fan duct. Only discrete points are available for static pressure at 124 degrees since it was only recorded on the high-speed digital recorder. Figure 3(b) indicates that the measured value of total pressure at 111 degrees is fairly uniform at all spanwise positions. As a further indication of a complicated asymmetric flow pattern present in the fan bypass-duct and afterburner, Fig. 3(c) illustrates that there exists a static pressure imbalance between right and left sides at station 8. Also included in this figure is the static pressure trace at station 9, which is located at the afterburner exit.

Evidence of an asymmetric flow pattern can also be observed by comparing total pressure traces at station 2.3 on the left and right sides of the engine, Figs. 3(d) and (e). On the left side, the total pressure is about equal to the static pressure in the bypass duct as indicated in Fig. 3(a). However, total pressure on the right side at 2.3-85-1 does not reach this level; instead, a large amplitude oscillation is seen to develop at this location. It should be noted that pressure transducer 2.3-85-1 is located directly under the splitter. Taking into account the large static pressure difference between bypass and core streams on this side of the engine, Figs. 3(a) and (e), the most likely cause for the oscillation at 2.3-85-1 is flow separation under the splitter. Figure 3(f) indicates that the total pressure oscillation at 2.3-85 is much smaller close to the hub, although the total pressure level is about the same. Although there was no instrumentation on the left side of the engine at station 2.3F, the indicated total pressure level on the left side of the engine at station 2.3 suggests that the flow breakdown at 2.3F occurs only on the right side.

Since this transient involves wave-propagation phenomena, it is of interest to relate the properties of the observed compression wave in the bypass duct to a one-dimensional discontinuous wave calculated assuming quasi-steady conservation equations. The pressure ratio for zero flow velocity behind the compression wave is given by:

$$\frac{P_{S2}}{P_{S1}} = 1 + \gamma M_1 \left[ \frac{\gamma + 1}{4} M_1 + \sqrt{\left( \frac{\gamma + 1}{4} M_1 \right)^2 + 1} \right]$$

where indices 1 and 2 refer to the conditions ahead of and behind the wave, respectively. For $M_1 = 0.24$, corresponding to the pretransient Mach number at station 2.3F, the pressure ratio is 1.39. At least during the initial pressure rise between 0.015 and 0.035 seconds in Fig. 3(a), this pressure ratio is not exceeded. The estimated value from the figure is about 1.32. The difference, however, is not a large one so that even on the basis of this simplified approach one might expect some complications in the flow structure in the bypass duct.

## Analysis of Pressure History During Stall

In this section stall pressure traces presented in Fig. 3 will be analyzed. (A summary of the stall history for other points will be presented in another section.) In the compressor stability analysis rotating stall is frequently encountered. It is characterized by appearance of either a periodic depression or a periodic peak in a pressure trace. Its time of occurrence will be assumed to correspond to either a maximum or a minimum pressure, since in this way arbitrariness associated with determining the point at which pressure starts rising or falling is avoided. It should be noted that the pressure pulse indicated in Fig. 3(d) in the trace 3.12-268-1 at about 0.040 sec does not appear to be related to the phenomena investigated here. This type of pressure pulse was also noticed prior to afterburner ignition. The time period was about 0.070 second. Similar oscillations were also noticed in the main burner static pressure trace.

Perhaps the most noticeable event preceding complete flow breakdown (abrupt stall) at about 0.122 sec is a spiked depression at location 2.3-85-1 at 0.111 sec, Fig. 3(e). At about the same time, pressure minima are observed at locations 3-118-3 and 3.12-82-2 which are closely aligned in axial direction (i.e., their circumferential orientation is about the same). Since these depressions in total pressure traces appear to be periodic, it is believed that they are due to rotating stall. Comparing total pressure traces 3-118-3, 3-118-1, and 3-262-2 in Figs. 3(d) and (e), it can be seen that stall at the low pressure compressor exit is initially confined to the hub portion of the blade span. Although not included, pressure trace 3-118-2 was also examined; it too did not indicate presence of stall. Referring to the total pressure traces 2.3-85-1, 2.3-265-2, and 3-118-3, it is seen that rotating stall is present at both, inlet and exit of the low pressure compressor; however, there is no indication of stall in the blade tip trace at 2.6-88-1. It is likely therefore, that stall at this location is also confined to the blade hub region. In view of this evidence, it is apparent that for the early detection of rotating stall it is essential to place total pressure instrumentation at different spanwise positions.

In order to determine periodicity and the speed of propagation of the rotating stall, the angular positions of stall cells are plotted in Fig. 4. (Some points in this plot were offset for clarity; their actual positions are indicated by using pointers.) In addition to the already mentioned locations, stall is believed to be detected at locations 2.3-111 and 3.12-268-1, so that these points are included in the figure. As indicated in Fig. 4, two diametrically opposed rotating stall cells (A and B) were assumed. The slope of the line faired through the points indicates that the speed of propagation of these two cells is 39 percent of low rotor speed. This is fairly close to the range of 43 to 57 percent reported in Ref. 4 for multistage compressors. It is interesting to note that following the abrupt stall, rotating stall could be detected throughout the compressor with the speed of propagation of about 40 to 45 percent of low rotor speed. If points in Fig. 4 were plotted assuming only one rotating stall cell, the resulting speed of propagation would be about 70 to 80 percent of low rotor speed. Only one stall cell at 2.3-265-2 is seen to complete one full revolution. Coincident with its second appearance, at 0.125 sec, abrupt stall is initiated. It extends axially throughout the left side of the engine, Fig. 3(d). Initiation of abrupt stall on the right side, as seen in Fig. 3(e), occurs about 3 milliseconds earlier. Again, abrupt stall is initiated almost simultaneously at axially aligned locations. In the high-pressure compressor, abrupt stall is initiated by a sudden drop in total pressure to a level approximately equal to the value of static pressure. In the low pressure stages, abrupt stall is initiated by a steep pressure rise followed immediately by a pressure drop. It appears that the abrupt stall represents a final stage of instability, whereas rotating stall represents a mechanism by means of which instability is propagated throughout the compressor system. It can also be observed in Fig. 3(e) that a compression wave resembling in appearance and strength the engine-inlet hammershock is detected only behind the first rotor. This supports the previously made observation (Ref. 5) that the strength of the hammershock is not related to overall compressor pressure ratio, being primarily a function of engine inlet Mach number. Here and in the subsequent discussion, the term hammershock will be used to denote a compression wave of about the magnitude necessary to stop the flow (Ref. 5) and should not be confused with small pressure spikes which sometimes appear before the abrupt stall.

## Analysis of Temperature Data

Because of relatively low thermocouple dynamic response, temperature data cannot be used for stall analysis; however, they can be used in conjunction with pressure data for the purpose of constructing the flow pattern during pre- and post-stall periods. Temperature histories for the ignition transient, point 23, are presented in Fig. 5. Since temperatures were recorded on the digital recorder, they were available only every 0.05 sec. In Fig. 5, the discrete points were connected by straight lines. The time scales in Figs. 3 and 5 are different. The point in time when peak temperature is reached at several locations in Fig. 5 (point C) corresponds to 0.134 sec in Fig. 3. Therefore, it appears that this temperature rise occurs as a result of stall.

In order to analyze the temperature plots in Fig. 5, it is instructive to compute total temperature rise across a discontinuous compression wave. Once again, one-dimensional quasi-steady conservation equations can be used to derive the following expression for the total temperature ratio:

$$\frac{T_2}{T_1} = 1 + \left\{1 - M_1\left[1 + \left(\frac{P_{S2}}{P_{S1}} - 1\right)\frac{\gamma + 1}{2\gamma}\right]^{-1/2}\right\}\left(\frac{P_{S2}}{P_{S1}} - 1\right)\frac{\gamma - 1}{\gamma}\left(1 + \frac{\gamma - 1}{2}M_1^2\right)^{-1}$$

This expression was derived without any restriction on the gas flowing behind the wave. For a pressure ratio of 1.32 estimated from Fig. 3(a) and a value of $M = 0.24$, the temperature ratio from this ex-

pression is about 1.07. In Fig. 5, the temperature ratio prior to stall at station 2.3F, $T_B/T_A$, is at most 1.037. Although the difference is significant, it is seen that this equation does yield a correct order of magnitude for the temperature difference due to compression. Referring to post-stall pressure histories in Figs. 3(e) and (d), it is also apparent that steep temperature rise observed in Fig. 5 between points B and C cannot be due to compression, and therefore, must be due to convective motion caused by the reverse flow during the post-stall period. The peak temperature at station 2.3F is somewhat lower than the peak temperature at the same circumferential position at station 2.3. It appears, therefore, that the post-stall temperature rise at 2.3F is due to the flow from the compressor core into the bypass duct. Figure 3(a) indicates that at this time, i.e., 0.134 sec, the flow direction is positive at 2.3F. It is significant to note that from the analysis of temperature data there is no indication of ingestion of afterburner exhaust gases at station 2.3F in either pre- or post-stall period.

Temperatures were plotted at two radial positions in Fig. 5 in order to illustrate variations in temperature at each station. It is seen that significant radial temperature difference exists at stations 3 and 4 prior to stall. Temperatures are higher at the hub at station 3, which is in qualitative agreement with higher pressures at the hub at this location noted in Fig. 3(d). It should be noted that in Fig. 5, corrections for thermocouple dynamic response, radiation, and recovery were not applied. It is estimated, however, that these corrections would not change in a significant way the reported temperature plots.

## Results for Additional Test Points

In this section, a summary of results will be presented for ignition transient point 24 (Fig. 2), three afterburner shut-down transients, 21, 22, and 27, and two transients, points 25 and 28, which did not result in stall. The essential features of the flow field in the bypass duct for point 24 are the same as noted previously for point 23, i.e., following ignition, total pressure on the right side of the engine at 2.3F drops below the static pressure level and a large-amplitude oscillation develops at 2.3-85-1. However, some differences can be observed in the stall history which is summarized in Fig. 6. The most significant difference is that in Fig. 6 rotating stall is correlated by assuming only one stall cell. The speed of propagation is 41 percent of low rotor speed, which is very close to the value of 39 percent obtained from Fig. 4, where two rotating stall cells were assumed. The distinction between rotating and abrupt stall is not so clear in this case. At about 0.117 sec, coincident with the last group of points in Fig. 6, there is a very steep pressure rise at location 2.1-282-3. At this time, stall is very strong on the left side. There is only partial recovery from rotating stall in the high pressure compressor, yet the complete flow breakdown on this side of the engine does not take place prior to 0.122 sec, and on the right prior to 0.120 sec. The temperature plots for this point are quite similar to those for point 23.

The prestall history of the afterburner shutdown transient is in many respects similar to prestall history of the ignition transient. Static pressure imbalance of similar magnitude develops in the afterburner at station 8; total pressure drops below the static pressure at 2.3F-111; and large fluctuations in total pressure are observed under the splitter. Preceding the formation of rotating stall, a drop in total pressure at 2.3-85-1 could be detected in all three cases. It is more pronounced for points 21 and 22 which correspond to lower Reynolds number indices. Static and total pressure traces under the splitter are presented for point 21 in Fig. 7 and a summary of stall history is given in Fig. 8(a). It can be observed from these figures that rotating stall is initiated under the splitter as a single cell. Subsequently, another stall cell is initiated in the low pressure compressor. Similarly as for point 24, a very strong rotating stall throughout the compressor (at about 0.137 sec in Fig. 7) is coincident with a steep pressure spike at 2.3-111 which indicates complete breakdown of flow at this location.

Rotating stall histories for points 22 and 27 are given, respectively, in Figs. 8(b) and (c). There is evidence of two stall patterns in both although in Fig. 8(c) the second stall cell appears only once, just before the abrupt stall. The abrupt stalls for these two points are observed first on one side of the engine and within two to three milliseconds on the other side. Comparing plots in Figs. 8(a) to (c), the most significant difference appears to be in the time interval between the first and last occurrence of rotating stall. It is considerably longer for point 21 for which the Reynolds number index is the lowest (Fig. 2). It is noted that dependence of this time on Reynolds number is closely related to the particular transient. For example, for the ignition transients 23 and 24, Reynolds number indices were lower than for point 21, although the time intervals between first and last occurrence of rotating stall are shorter for these two test points (Figs. 4, 6, and 8(a)). Rotating stall speed for test point 21 is about 38 percent of low rotor speed and for points 22 and 27 it is about 36 percent of low rotor speed.

The additional evidence presented in this section, particularly for test points 21 and 24 (Figs. 8(a) and 6), indicates that stall appears first in the region under the splitter. It is not clear, however, whether stall origin is in the last two fan-hub stages or in the first few stages in the low pressure compressor. Rotating stall is propagated through the low pressure compressor first and then through the high pressure compressor. Abrupt stall is initiated usually within 10 milliseconds of the appearance of rotating stall in the high pressure compressor.

Temperature plots were also obtained for transients 21, 22, and 27. Again, there was no evidence of ingestion of afterburner exhaust gases into the bypass duct. In addition, pressure and temperature traces were examined for two points just to the right of the respective stall boundaries in Fig. 2, i.e., points 25 and 28. All essential features of the internal flow field prior to stall described for each transient could also be noted for these two points. For example, Fig. 9 illustrates pressure history under the splitter during afterburner ignition for point 25. It is apparent, therefore, that flow reversal at station 2.3F as well as flow separation under the splitter do not necessarily lead to compressor stall. A necessary condition is that Reynolds number index be sufficiently low. The only temperature rise noted at station 2.3F was due to compression wave. It is significant to note that there was no indication of rotating stall for these two points. It appears, therefore, that rotating stall in the operating range close to Military necessarily leads to a complete flow breakdown. This is in contrast with the low speed operating range where rotating stall can be maintained without severe degradation of performance.

## CONCLUDING REMARKS

1. At a simulated high altitude and a flight Mach number of 1.3 flow breaks down in the bypass duct at the fan discharge as a result of afterburner ignition and shutdown transients. This occurs only on one side of the engine and is always followed by a large total pressure fluctuation under the core-bypass splitter ring on the same side.

2. Compressor stall occurs during the ignition transient when engine inlet Reynolds number index drops below 0.23, and during the shut-down transient when the Reynolds number index drops below 0.34.

3. Complete compressor stall was always preceded by a rotating stall. Rotating stall was not detected during either transient outside respective stability boundaries.

4. Rotating stall is most frequently detected first under the splitter, and last in the high pressure compressor.

5. Rotating stall at the exit of low pressure compressor originates at the hub.

6. Consistent results on the speed of propagation of the rotating stall could only be obtained by assuming a two-cell rotating stall pattern in four out of the five cases analyzed. The speed of propagation of the rotating stall was found to be between 36 and 41 percent of low rotor speed.

7. The time interval between first and last detected occurrence of rotating stall varied between 17 and 50 milliseconds. For the shut-down transient this time depends on the Reynolds number index.

8. Post-stall hammershock could be detected behind the first fan rotor, but there was no indication of hammershock at any of the downstream stations.

## REFERENCES

1. McAulay, John E.; and Abdelwahab, Mahmood: Experimental Evaluation of a TF30-P-3 Turbofan Engine in an Altitude Facility: Afterburner Performance and Engine-Afterburner Operating Limits. NASA TN D-6839, 1972.

2. Armentrout, Everett C.: Development of a High-Frequency Response Pressure-Sensing Rake for Turbofan Engine Tests. NASA TM X-1959, 1970.

3. Braithwaite, Willis M.; Dicus, John H.; and Moss, John E., Jr.: Evaluation with a Turbofan Engine of Air Jets as a Steady-State Inlet Flow Distortion Device. NASA TM X-1955, 1970.

4. Aerodynamic Design of Axial Flow Compressors. NASA SP-36, 1965, pp. 311-330.

5. Kurkov, Anatole P.; Soeder, Ronald H.; and Moss, John E., Jr.: Investigation of the Stall Hammershock at the Engine Inlet. J. Aircraft, vol. 12, no. 5, May 1975.

TABLE I. - LOCATION OF HIGH-RESPONSE PRESSURE TRANSDUCERS

| Pressure | Station | Circum. position, deg | Radial position | Passage height, percent | Pressure | Station | Circum. position, deg | Radial position | Passage height, percent |
|---|---|---|---|---|---|---|---|---|---|
| $P_S$ | 2 | 108 | | 100 | $P_t$ | 2.6 | 88 | 1 | 85.8 |
| $P_t$ | 2 | 90 | 2 | 78.2 | $P_S$ | 3 | 82 | | 100 |
| $P_t$ | 2 | 270 | 4 | 41.8 | $P_t$ | 3 | 118 | 1 | 85. |
| $P_S$ | 2.1 | 53 | | 100 | $P_t$ | 3 | 118 | 2 | 53.3 |
| $P_t$ | 2.1 | 282 | 3 | 59.1 | $P_t$ | 3 | 118 | 3 | 19.0 |
| $P_S$ | 2.3 | 111 | | 100 | $P_t$ | 3 | 262 | 2 | 69.2 |
| $P_t$ | 2.3 | 85 | 1 | 90.3 | $P_S$ | 3.12 | 69 | | 100 |
| $P_t$ | 2.3 | 85 | 4 | 20 | $P_t$ | 3.12 | 82 | 2 | 27.3 |
| $P_t$ | 2.3 | 265 | 2 | 69.3 | $P_t$ | 3.12 | 268 | 1 | 69.7 |
| $P_S$ | 2.3F | 124 | | 100 | $P_t$ | 4 | 76 | 2 | 26.6 |
| $P_t$ | 2.3F | 111 | 1 | 89 | $P_S$ | 4F | 90 | | 100 |
| $P_t$ | 2.3F | 111 | 2 | 65.7 | $P_S$ | 8 | 95 | | 100 |
| $P_t$ | 2.3F | 111 | 4 | 8.3 | $P_S$ | 8 | 270 | | 100 |
| $P_S$ | 2.6 | 69 | | 100 | $P_S$ | 9 | 95 | | 100 |

TABLE II. - LOCATION OF HIGH-RESPONSE THERMOCOUPLES

| Station | Circum. position, deg | Radial position | Passage height, percent |
|---|---|---|---|
| 2.3 | 56 | 2 | 78.5 |
| 2.3 | 56 | 3 | 61 |
| 2.3F | 56 | 2 | 71.8 |
| 2.3F | 56 | 4 | 34 |
| 2.6 | 130 | 1 | 91 |
| 2.6 | 130 | 5 | 12 |
| 3 | 58 | 1 | 91 |
| 3 | 58 | 5 | 12 |
| 4 | 120 | 1 | 90 |
| 4 | 120 | 5 | 10.5 |

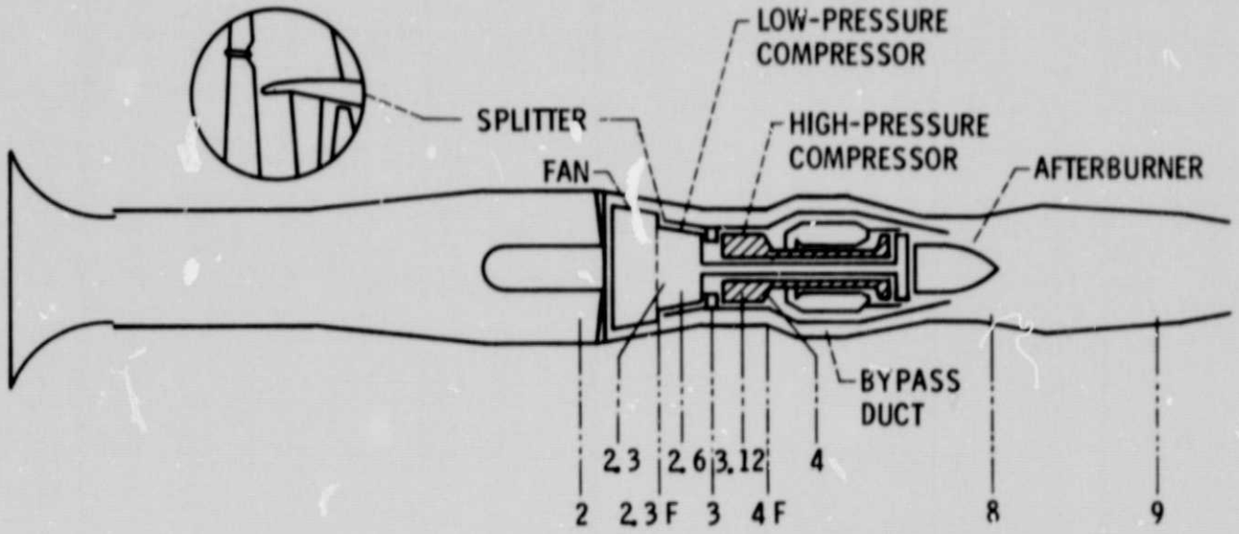


Figure 1. - Engine installation on instrumentation stations.

E-8375

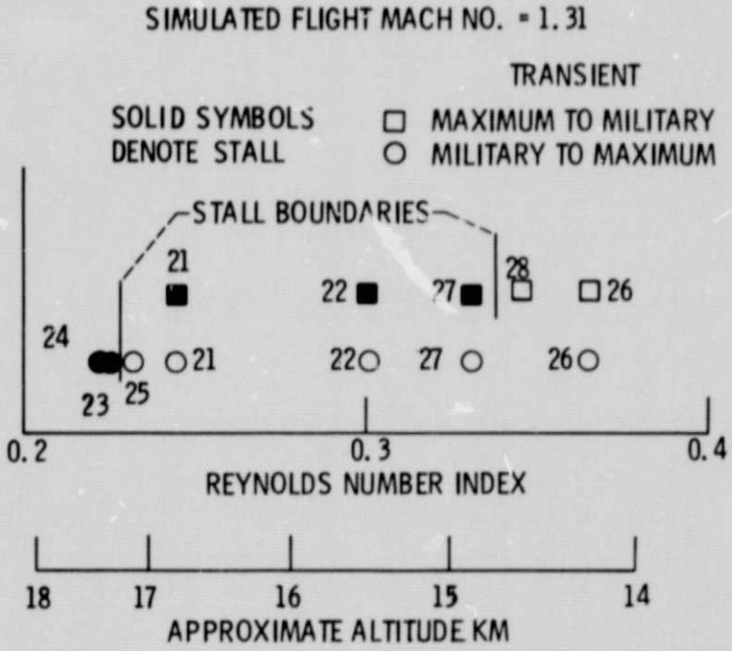


Figure 2. - Dependence of stall/no-stall boundaries on Reynolds number index during afterburner transients.

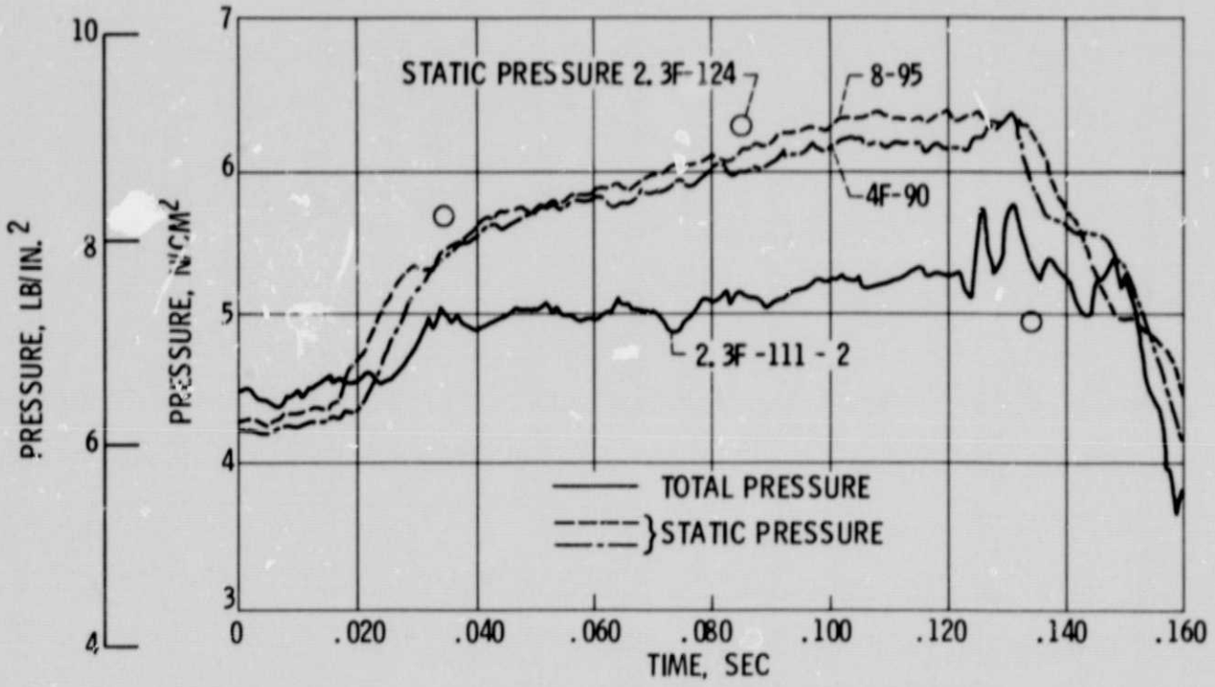


(a) AFTERBURNER AND FAN-DUCT PRESSURES.

Figure 3. - Pressure histories during stall for test point 23. Throttle movement from Military to Maximum.

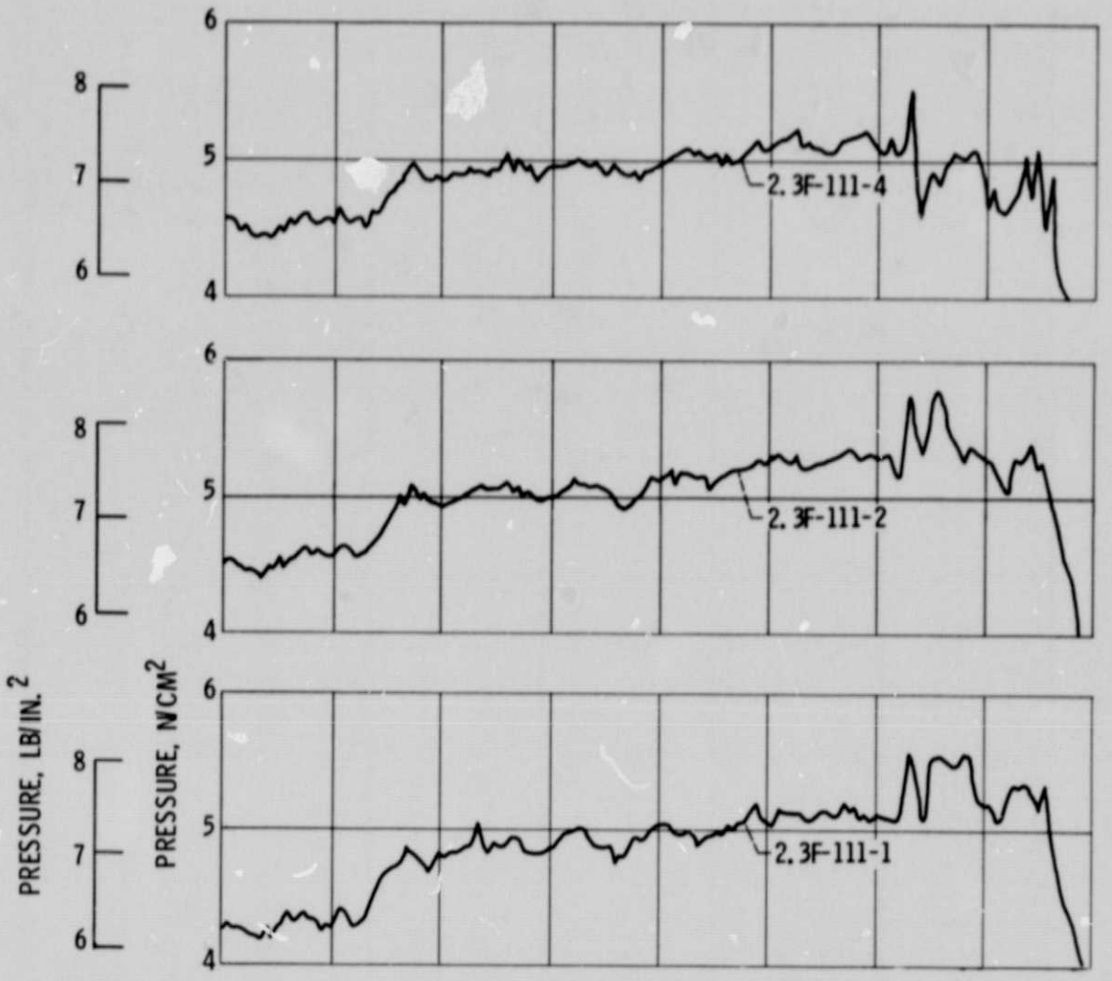


(b) FAN DISCHARGE TOTAL PRESSURES.

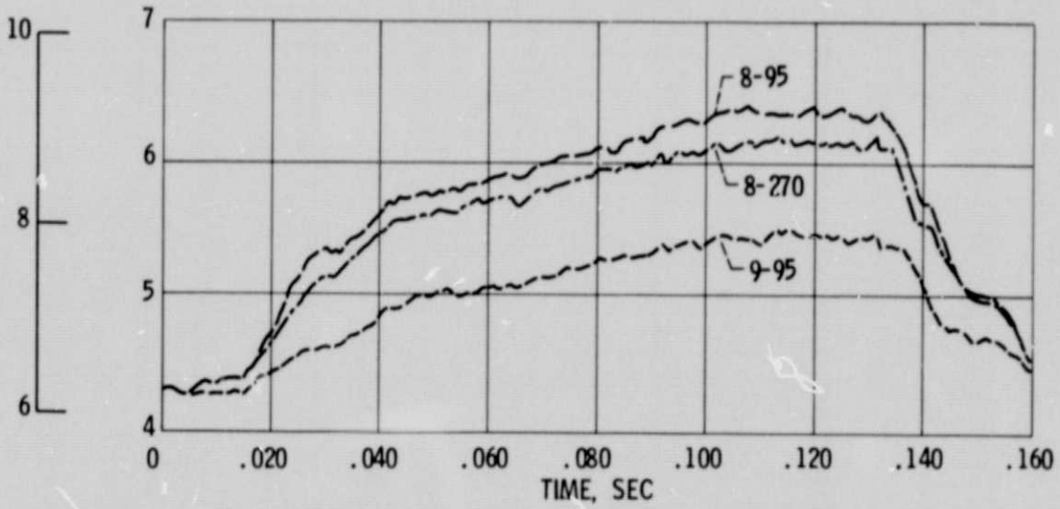


(c) STATIC PRESSURES IN THE AFTERBURNER.

Figure 3. - Pressure histories during stall for test point 23. Throttle movement from Military to Maximum.

E-8375

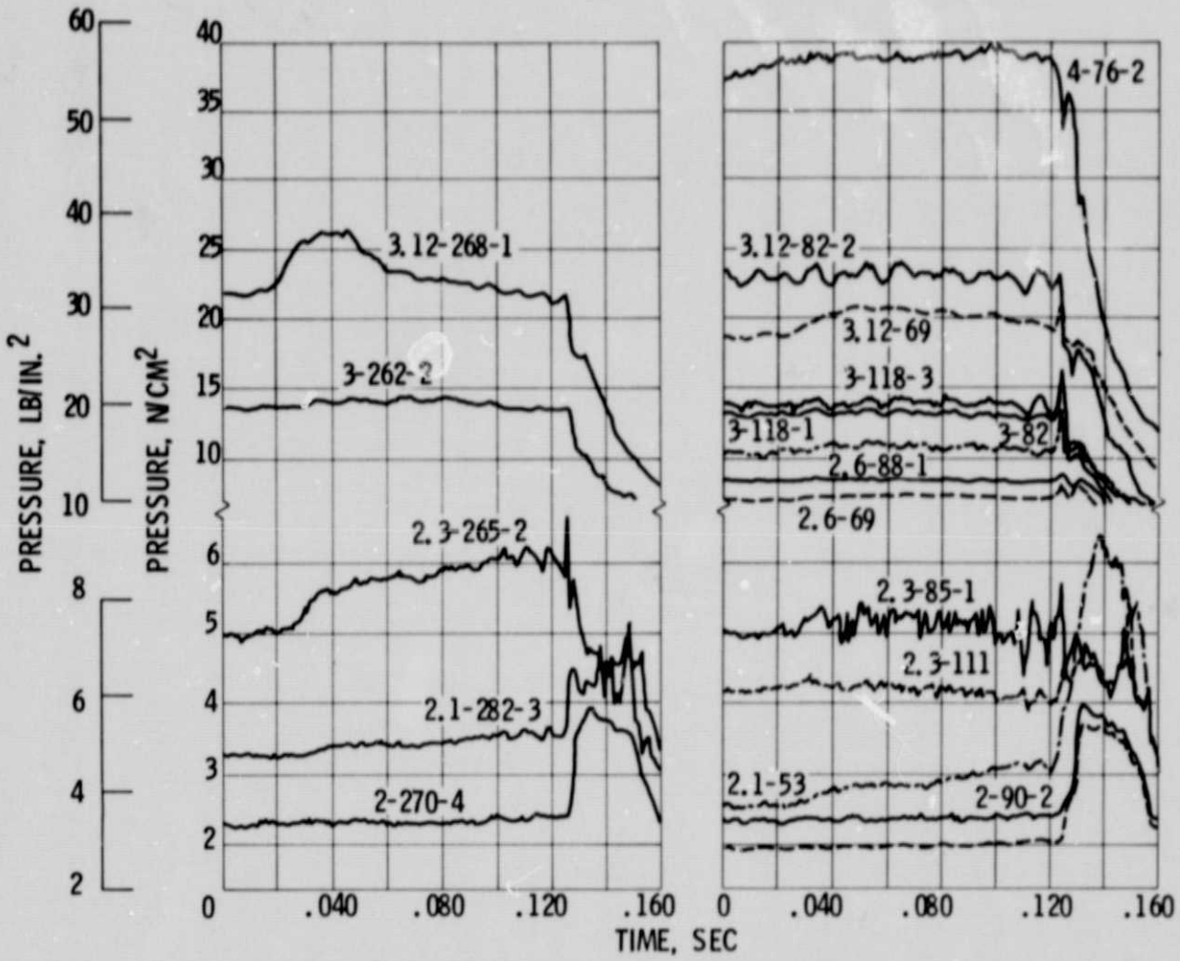


(d) TOTAL PRESSURES ON THE LEFT SIDE OF THE ENGINE.

(e) PRESSURES ON THE RIGHT SIDE OF THE ENGINE.

Figure 3. - Pressure histories during stall for test point 23. Throttle movement from Military to Maximum.

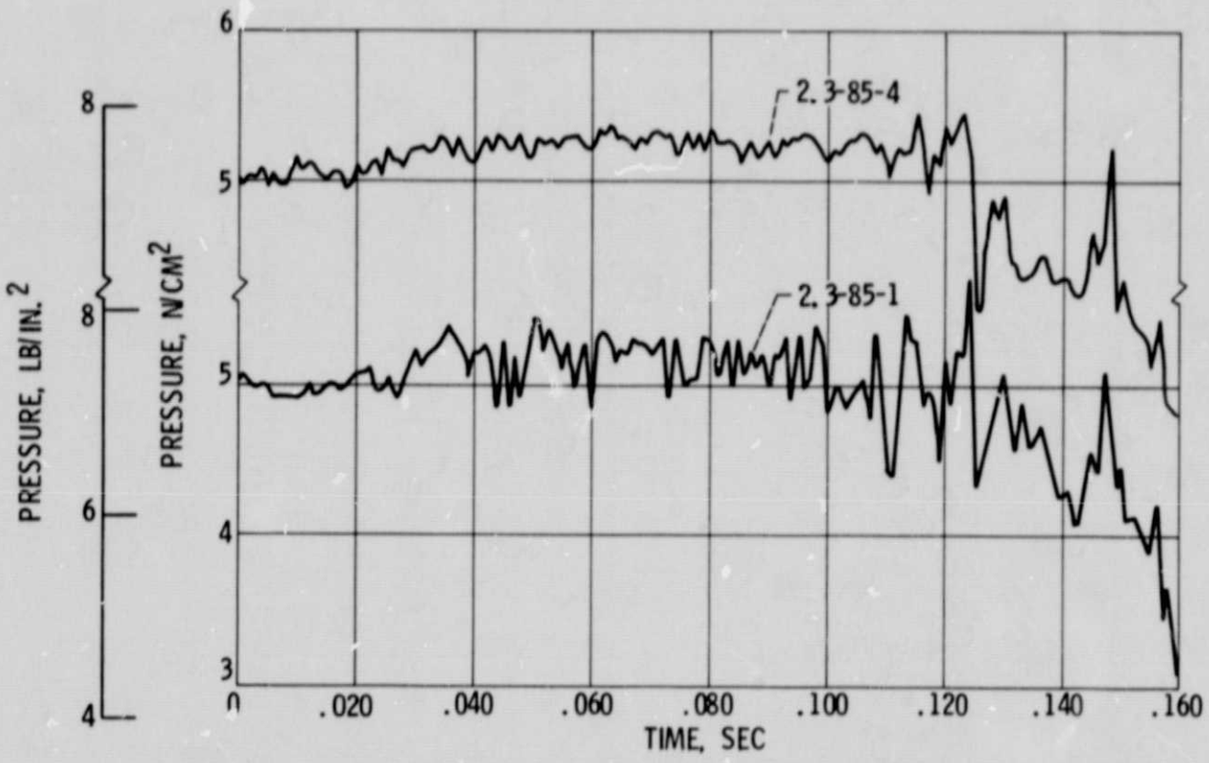


(f) LOW PRESSURE COMPRESSOR INLET.

Figure 3. - Pressure histories during stall for test point 23. Throttle movement from Military to Maximum.

E-8375

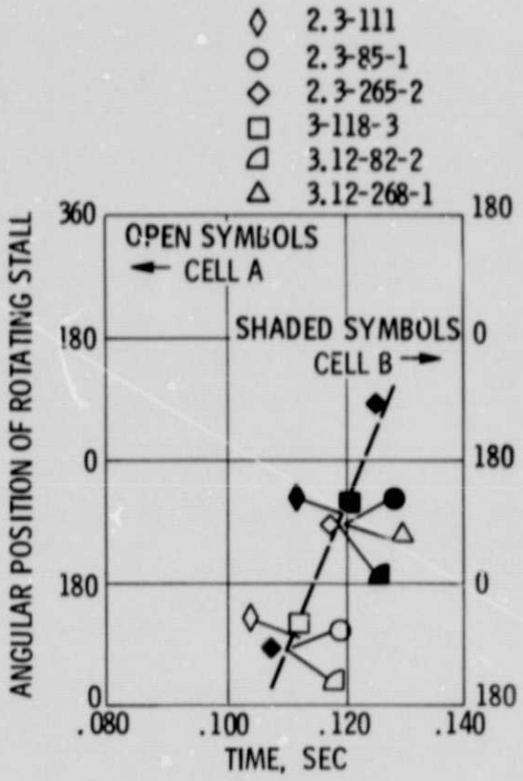


Figure 4. - Rotating stall history during throttle movement from Military to Maximum for test point 23.

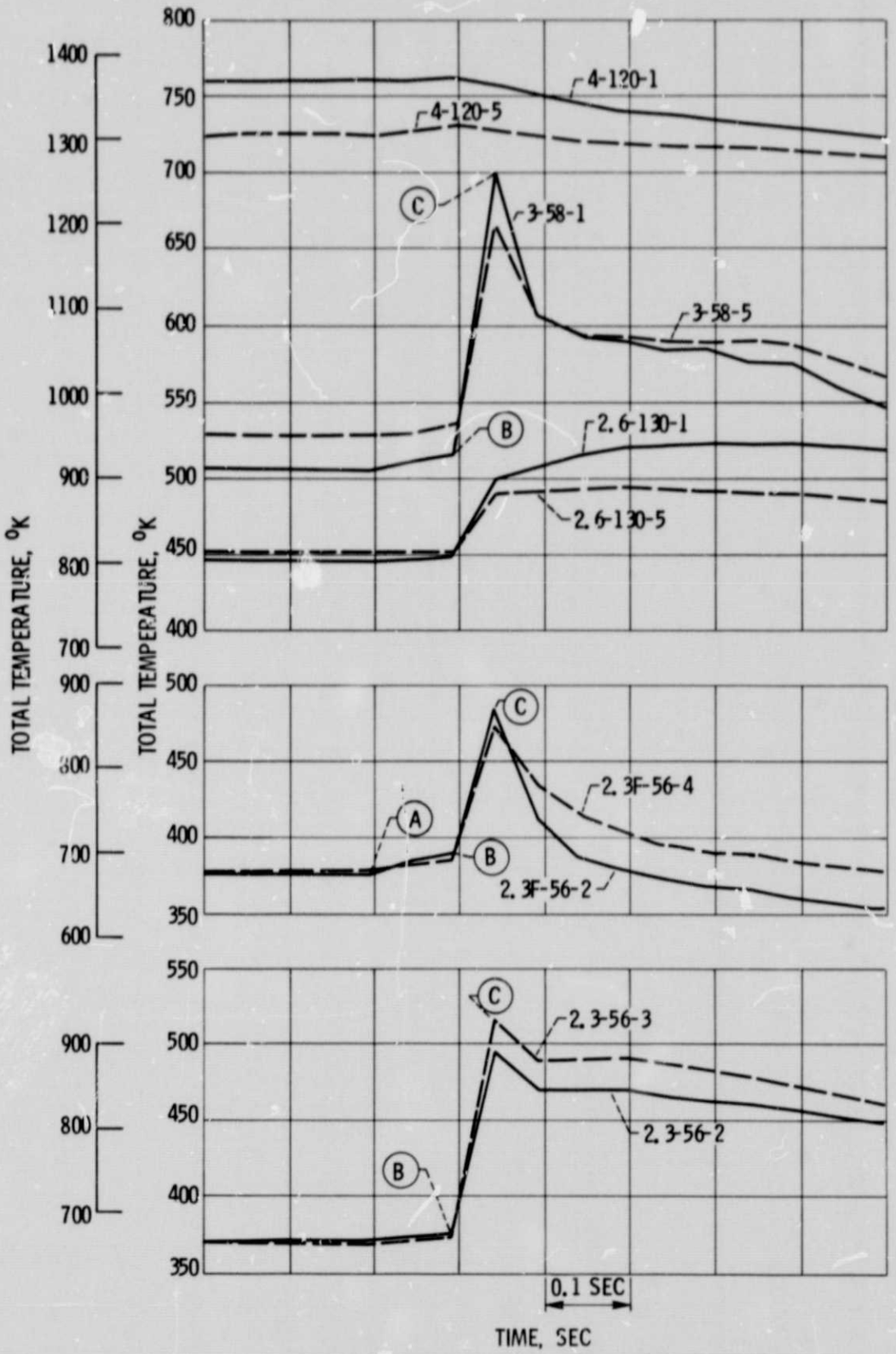


Figure 5. - Total temperature histories during stall for test point 23.

E-8375

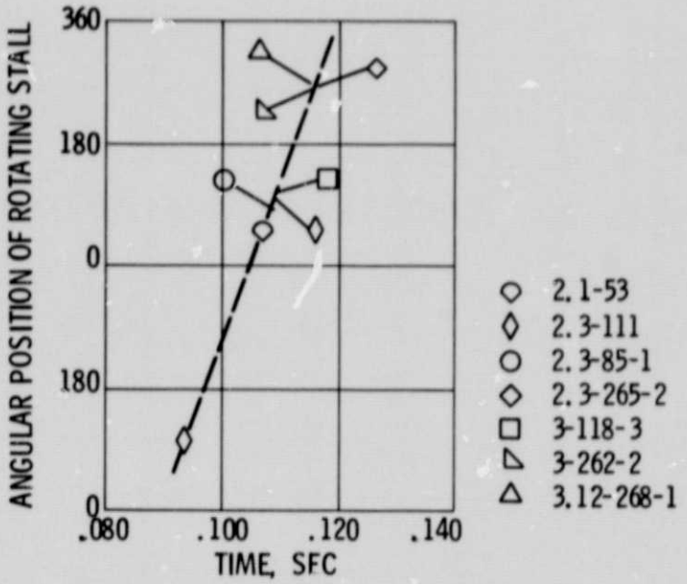


Figure 6. - Rotating stall history during throttle movement from Military to Maximum for test point 24.

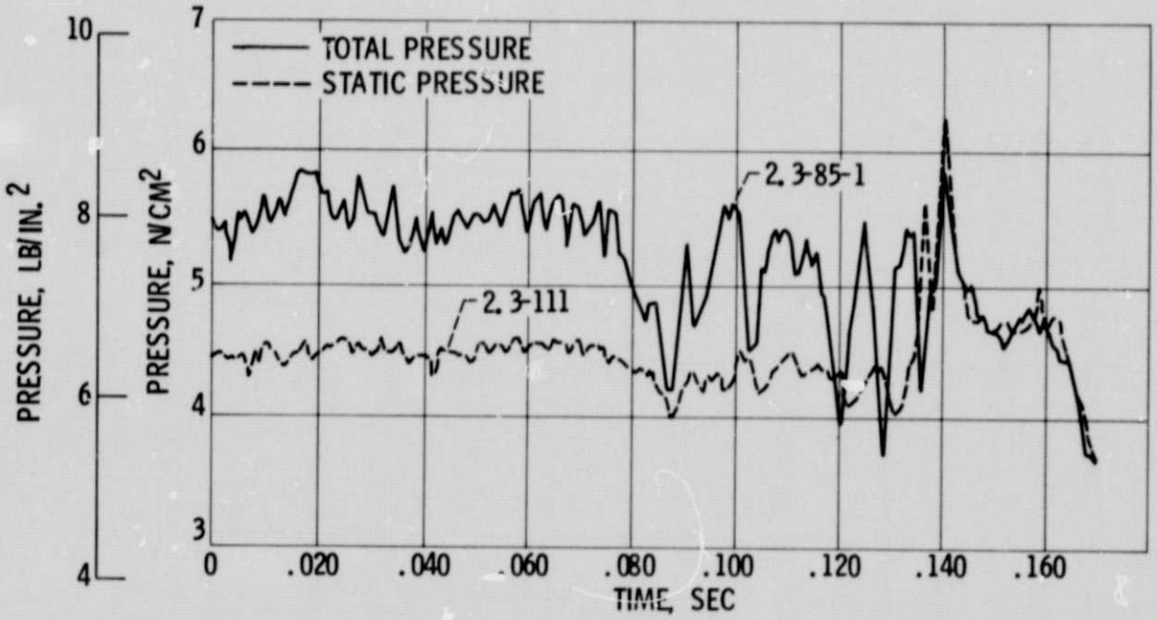


Figure 7. - Pressure histories at station 2.3 for test point 21. Throttle movement from Maximum to Military.

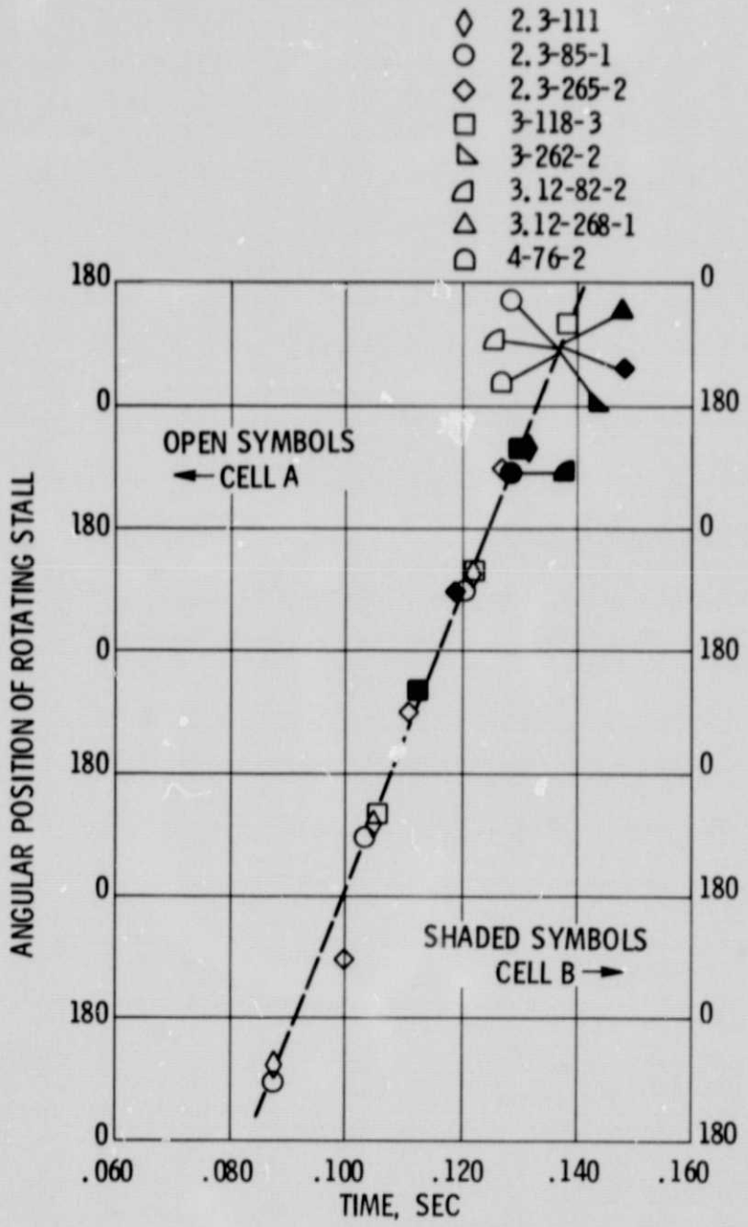


(a) TEST POINT 21.

Figure 8. - Rotating stall history during throttle movement from Military to Maximum.

E-8375

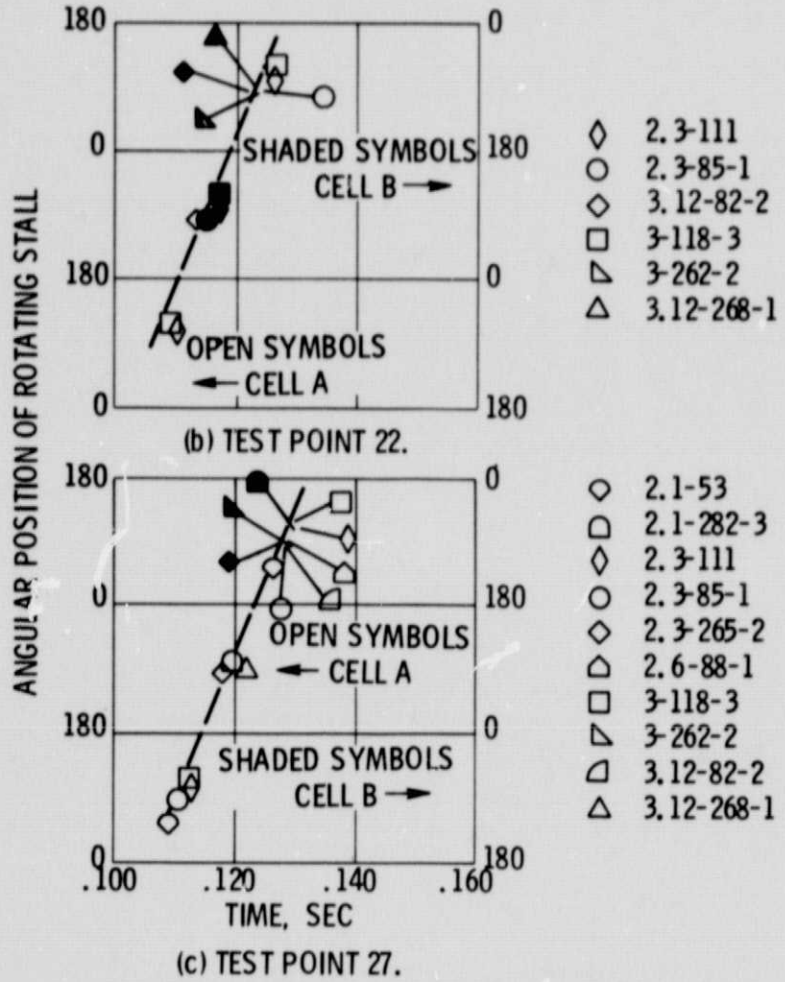


Figure 8. - Rotating stall history during throttle movement from Military to Maximum.

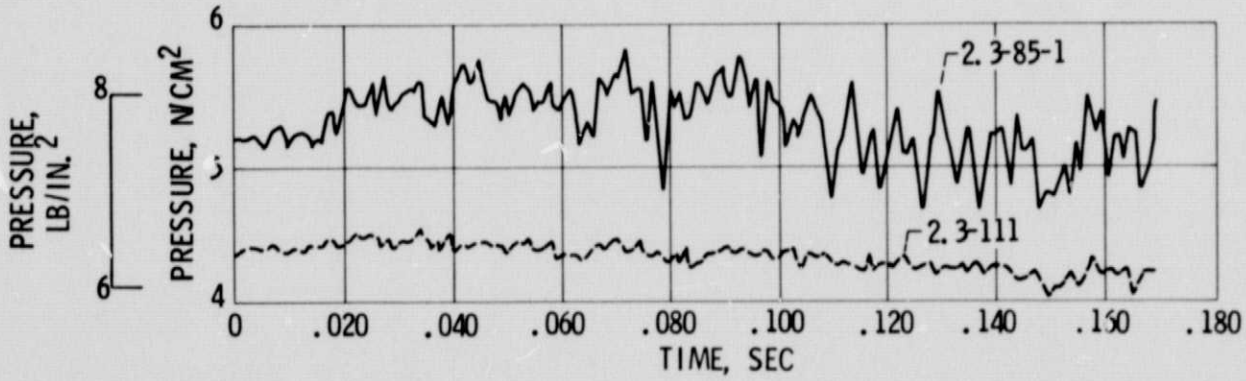


Figure 9. - Pressure history under the splitter for test point 25.